Small-Area Si Photovoltaics for Low-Flux Infrared Energy Harvesting

Eunseong Moon, *Student Member, IEEE*, David Blaauw, *Fellow, IEEE*, and Jamie D. Phillips, *Senior Member, IEEE*

***Abstract*— Silicon photovoltaics are prospective candidates to power mm-scale implantable devices. These applications require excellent performance for small-area cells under low-flux illumination condition, which is not commonly achieved for silicon cells due to shunt leakage and recombination losses. Small area (1–10 mm^2) silicon photovoltaic cells are studied in this paper, where performance improvements are demonstrated using a surface n-type doped emitter and Si_3N_4 passivation. A power conversion efficiency of more than 17% is achieved for 660-nW/mm^2 illumination at 850 nm. The silicon cells demonstrate improved power conversion efficiency and reduced degradation under low illumination conditions in comparison with conventional crystalline silicon photovoltaic cells available commercially.**

***Index Terms*— Energy harvesting, photovoltaics, shunt resistance, silicon.**

I. Introduction

HUMAN microchip implant [1]–[4] is a promising technology for a variety of applications, including identification, biomedical sensors for monitoring neuron pulses [5], biomarkers [6], and tracking positions [7]. Recently developed low power systems [8] have made implantable systems a feasible approach. Energy harvesting from vibration and RF sources [9] has been tested and evaluated, but the stability of the energy source and miniaturization is challenging [4], [9]. Alternatively, infrared photovoltaic energy harvesting has been considered, utilizing the near-infrared (NIR) transparency window of tissue between 700 and 1100 nm [10] from natural ambient sunlight or intentional low-intensity LED illumination through tissue. High-efficiency photovoltaic cells based on III–V semiconductors for mm-scale low-power systems under low-flux illumination may meet these requirements, where GaAs cells have achieved 19.4% power conversion efficiency under indoor 1-μW/mm^2 illumination [11].

One of the obstacles facing GaAs-based photovoltaic cells is concerns related to toxicity, despite encapsulation with biocompatible materials. Silicon photovoltaics may be a more attractive option for implantable devices due to their excellent NIR response, compatibility with silicon CMOS [12], and reduced cost. High-efficiency silicon photovoltaic cells are well established for solar energy, where low flux solar response has demonstrated a power conversion efficiency of 13.5% under 1 μW/mm^2 [13] and 13.1% under 3-μW/mm^2 AM 1.5 illumination [14]. However, specific requirements for the 700–1100-nm NIR window and mm-scale device size have not been addressed, where sidewall recombination [11], [15] and shunt resistance [13], [17] are expected to be critical. In this paper, mm-scale silicon photovoltaic cells are explored for low-flux NIR energy harvesting.

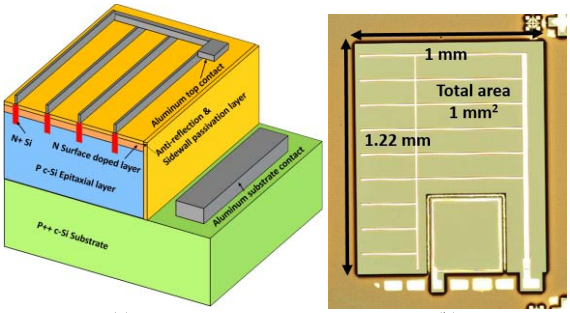

Fig. 1. (a) Schematic of device structure. (b) Optical microscope image of a fabricated 1-mm^2 device.

II. Experiment

Silicon photovoltaic cells were designed and simulated using Sentaurus Device [18], using built-in values for silicon material parameters at 300 K, as indicated in Table I, and neglecting the edge effects, including surface recombination and sidewall recombination. The baseline device structure consists of a thick p-type silicon base layer on heavily doped p-type silicon substrate and diffused n-type emitter contacts on the top surface, as shown in Fig. 1(a). The baseline geometry utilizing a heavily doped substrate and lightly-doped base, while unconventional for solar Photovoltaic (PV), is selected in this paper to provide top contacts to facilitate a stacked configuration for mm-scale systems [8]. A lightly-doped n-type emitter near the surface between heavily doped emitter contacts was also included for select samples with the goal of improving carrier collection. The base thickness and doping concentration were optimized for irradiation between 800 and 850 nm at a power density of 100 nW/mm^2.

Manuscript received September 20, 2016; revised October 27, 2016 and November 3, 2016; accepted November 4, 2016. Date of publication November 17, 2016; date of current version December 24, 2016. This work was supported by the National Science Foundation and the National Institutes of Health under Award R01CA195655. The review of this paper was arranged by Editor A. G. Aberle.

The authors are with the Department of Electrical Engineering and Computer Science, University of Michigan, Ann Arbor, MI 48109 USA (e-mail: esmoon@umich.edu; blaauw@umich.edu; jphilli@umich.edu).

Color versions of one or more of the figures in this paper are available online at http://ieeexplore.ieee.org.

Digital Object Identifier 10.1109/TED.2016.2626246

TABLE I
SILICON SIMULATION PARAMETERS AT 300 k

Parameter	Value	Unit
Bandgap	1.124	eV
Intrinsic carrier concentration	1.075×10^{10}	cm^{-3}
Refractive index	3.681 (at 800 nm) 3.65 (at 850 nm)	
Absorption coefficient	850 (at 800 nm) 535 (at 850 nm)	cm^{-1}
Carrier lifetime	10^{-5} (for electron) $3x10^{-6}$ (for hole)	s

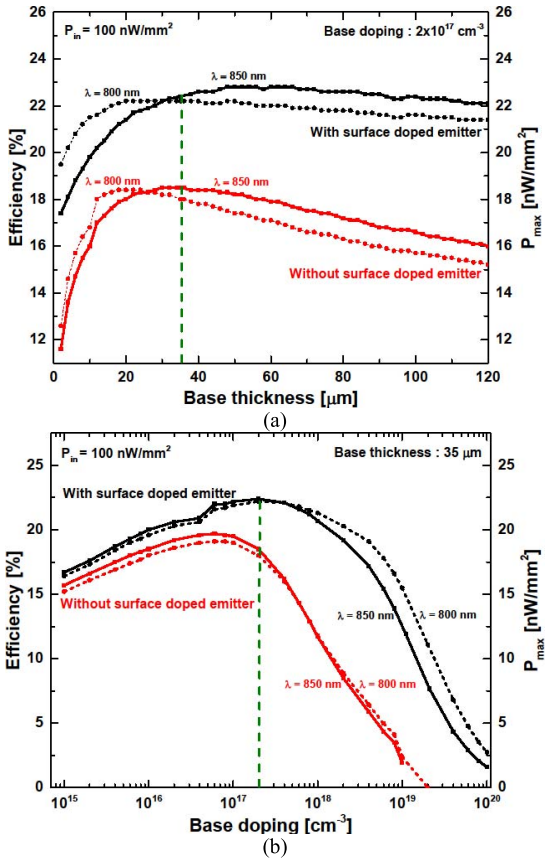

Fig. 2. Simulated power conversion efficiency under 100-nW/mm^2 illumination at 800 nm (dashed line) and 850 nm (solid line) for variable. (a) Base thickness. (b) Base doping concentration.

The dependence of power conversion efficiency on base layer thickness and doping concentration is shown in Fig. 2. Base thickness near 35 μm, corresponding to optical absorption depth [19] of silicon at 300 K, and base doping concentration near 2×10^{17} cm^{-3} were found to provide near optimal performance under the NIR illumination conditions simulated. The inclusion of a surface n-type emitter with thickness of 340 nm and concentration of 2.5×10^{16} cm^{-3} was found to significantly increase the power conversion efficiency, as shown in Fig. 2. Optimized device parameters are summarized in Table II.

TABLE II
OPTIMIZED DEVICE PARAMETERS UNDER ILLUMINATION OF 100 nw/mm^2 BETWEEN 800 AND 850 nm

Parameter	Value	Unit
Base thickness	35	μm
Base doping concentration	2×10^{17}	cm^{-3}
N-type surface layer thickness	0.34	μm
N-type surface layer doping	2.5×10^{16}	cm^{-3}
Anti-reflection Si_3N_4 layer	100	nm
Emitter width	3	μm
Emitter depth	0.46	μm

Devices were fabricated from epitaxial silicon wafers grown by chemical vapor deposition, with base thickness measured between 33 to 37 μm. The base doping concentration was 1.5×10^{16} cm^{-3}, corresponding to a resistivity of 1 Ω-cm. A lower base doping concentration than the optimal identified from simulations was used with the objective of reducing sensitivity to shunt resistance leakage paths. Emitter junctions and lightly doped surface emitter (for select samples) were formed via phosphorous diffusion. The thermal phosphorous doping process results in a Gaussian doping profile with an estimated junction depth around 1.5 μm. A lightly doped emitter with 1.2 μm thickness and 5×10^{18} cm^{-3} peak concentration was formed through a subsequent 300-nm reactive ion etch of the top surface. Aluminum contacts were fabricated for the n-type and p-type layers using conventional photolithography, electron beam evaporation, and wet chemical etching processes. Photolithography and reactive ion etching were used for device isolation and patterning to contact the heavily doped p-type substrate. Due to the strong sidewall/perimeter dependence of small area PV cells [11], [15], variable device area was studied in the range of 0.02 to 10 mm^2, corresponding to a perimeter/area (P/A) ratio from 35.84 to 1.4 mm^{-1}. Several sidewall and surface passivation layer processes were investigated, since surface recombination is expected to have a major impact on device performance for small mm-scale devices operating under low-flux conditions [11], [15]. Passivation layers studied in this paper include low-pressure chemical vapor deposition (LPCVD) of Si_3N_4, LPCVD a-Si, and SiO_2 via dry thermal oxidation, plasma-enhanced chemical vapor deposition (PECVD) of Si_3N_4 and PECVD SiO_2, and no passivation for comparison. Further details on the six different passivation layers under study: 1) 50-nm LPCVD Si_3N_4 (refractive index: 2.02) at 800 °C +50-nm PECVD Si_3N_4 at 380 °C; 2) 25-nm LPCVD a-Si at 560 °C + 100-nm PECVD Si_3N_4 at 380 °C; 3) 40 nm thermally grown dry SiO_2 at 900 °C +50-nm LPCVD Si_3N_4 at 800 °C + 100-nm PECVD SiO_2 at 380 °C; 4) 100-nm PECVD Si_3N_4 at 380 °C; 5) 100-nm PECVD SiO_2 at 380 °C; and 6) control sample without passivation.

Electrical current density versus voltage (J–V) characteristics under dark and illumination were measured using a Keithley 4200 Semiconductor Characterization System.

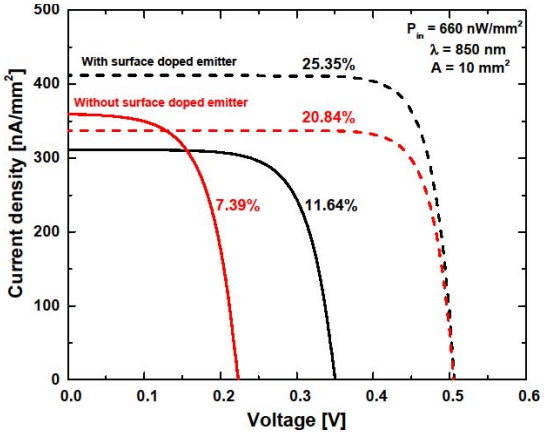

Fig. 3. Measured (solid line) and simulated (dashed line) current–voltage characteristics of silicon photovoltaic cells with thermal SiO_2 passivation and with/without lightly doped emitter under 660-nW/mm^2 illumination at 850 nm.

Low-flux illumination conditions were controlled by a microscope-compatible 850-nm infrared light emitting diode and calibrated power meter. Power conversion efficiency was measured for irradiation at a power density of 660 nW/mm^2, which is extremely dim in comparison with the power density of AM 1.5 sunlight of 1000 μW/mm^2 [20]. The external quantum efficiency spectrum was measured on select samples using a system equipped with a halogen white light source, lock-in amplifier, monochromator, and calibrated photodetector.

III. Results

A. Surface Doped Emitter

The impact of the lightly doped surface emitter on device performance is illustrated by the response under IR illumination and under dark conditions, as shown in Figs. 3 and 4. The IR power conversion efficiency is dramatically increased from 7.39% to 11.64% (Fig. 3) for a 10-mm^2 cell. The short circuit current density (J_{SC}) of the cell with surface n-type emitter was reduced in contrast to the simulation results, due to the nonideal Gaussian doping profile of the surface emitter with peak concentration near 10^{20} cm^{-3}. This heavily doped surface layer introduces free carrier absorption and degradation in carrier lifetime, thus reducing J_{SC}. A majority of the improved power conversion efficiency is attributed to an increase in open circuit voltage (V_{OC}), suggesting a corresponding reduction in the reverse saturation current (J_0). The n-type emitter alters the field-effect passivation between silicon and thermal SiO_2 from inversion to accumulation, resulting in dramatic improvements in the carrier lifetime at low carrier injection [21] and reduction in the reverse saturation current. Dark current measurements demonstrate a decrease in the reverse saturation current density [Fig. 4(a)], agreeing with the increased value of V_{OC}. Numerical parameters for dark current were obtained by fitting the forward biased region from 0 to 0.4 V to the diode equation

$$J = J_0\left[\exp\left(\frac{qV}{nkT}\right) - 1\right] \quad (1)$$

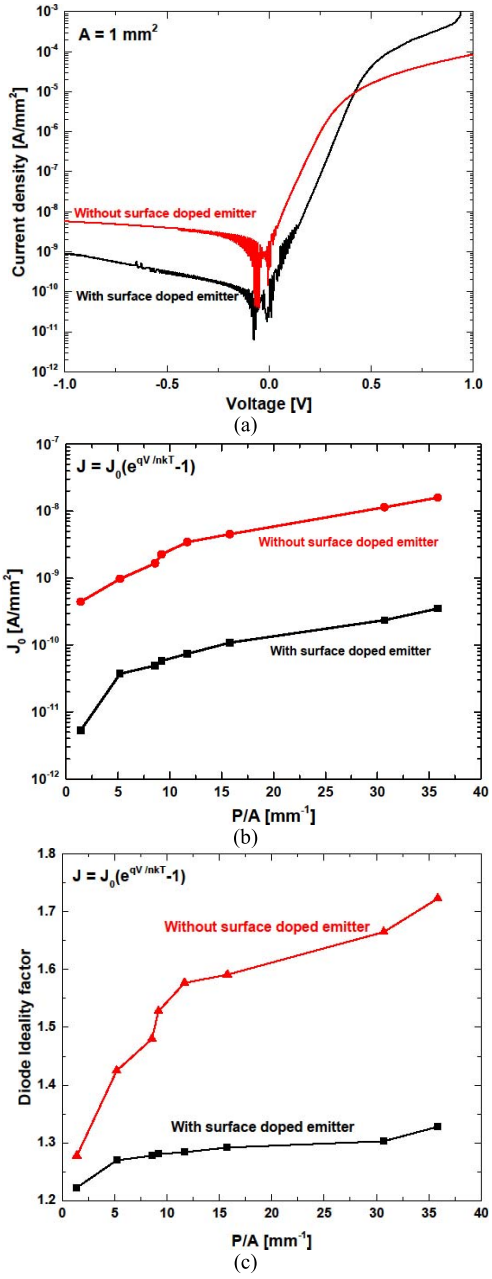

Fig. 4. (a) Measured current versus voltage characteristics of cells with thermal SiO_2 passivation and with/without lightly doped emitter under dark conditions. (b) Extracted J_0 parameters and (c) diode ideality factors versus P/A (mm^{-1}◁ ratio from 1.4 to 35.84 mm^{-1} corresponding device size from 10 to 0.02 mm^2.

where J is the total current density, V is the applied voltage, n is the diode ideality factor, k is the Boltzmann constant, T is the temperature, and J_0 is the reverse saturation current. Extracted parameters for J_0 [Fig. 4(b)] demonstrate a strong perimeter dependence, ranging from 5.31 to 348.96 pA/mm^2 for the surface doped sample and from 0.443 to 15.9 nA/mm^2 for a cell without the surface doped emitter layer. In all the cases, the cell with a surface n-type emitter demonstrates a decrease in J_0 by one to two orders of magnitude. The extracted ideality factor also emphasizes the improvement in device performance with the inclusion of the surface

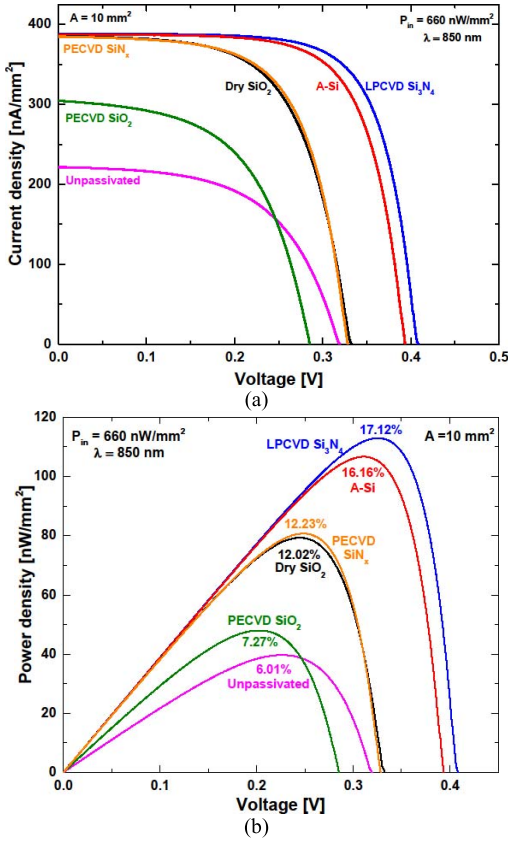

Fig. 5. (a) Measured current versus voltage characteristics. (b) Power density versus voltage of different passivation layers and 10-mm^2 cell under 850-nm LED illumination with 660 nW/mm^2.

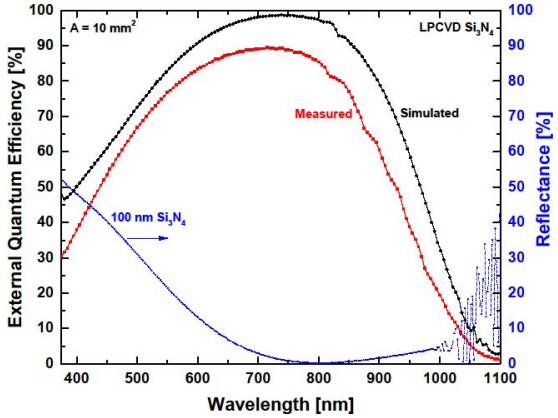

Fig. 6. Measured and simulated EQE characteristics for the 100-nm LPCVD Si_3N_4 passivated cell along with a surface reflectance curve (dashed line) of cell between 375- and 1100-nm wavelength.

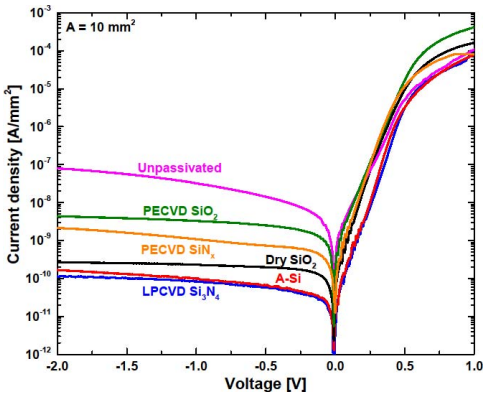

Fig. 7. Measured *J–V* under dark conditions for samples with different passivation layers.

n-type emitter. The ideality factor for the sample without the surface doped layer demonstrates a strong dependence on P/A ranging from 1.285 to 1.723, while the ideality factor of the surface doped sample only shows a relatively small increase from 1.223 to 1.303. This unwanted increase in the diode ideality factor for the sample without the surface n-type emitter is attributed to an increase in Shockley–Read–Hall recombination in the space charge region near the surface due to surface inversion at the p-Si and SiO_2 interface [21]. While the surface doping technique demonstrates substantial improvements in the power conversion efficiency, the measured values are still substantially lower than simulated values. The primary source of efficiency reduction is likely due to nonideal thermal silicon dioxide passivation of the p-type sidewall resulting in reduced minority carrier diffusion length. Improved passivation of the sidewall may be achieved by using a-Si or Si_3N_4 [21] to approach the simulated efficiency values. Losses associated with the high doping concentration at the emitter surface interface, such as free carrier absorption or Auger recombination, are other efficiency limiting factors. An optimized doping profile of the surface n-type emitter through selective etching between the light harvesting and metal finger regions is required, as well as improved design of the surface passivation layer to serve as an antireflection coating and layer to effectively reduce bulk and sidewall recombination losses.

B. Passivation Layer

Silicon cells with variable passivation layers and optimized surface n-type emitter were fabricated. The passivation layers served the dual purpose of an antireflection coating, where the surface reflectance was optimized at a wavelength of 800 nm. The 100-nm Si_3N_4 is expected to provide 1%–2% surface reflectance at 850 nm, as shown in Fig. 6. Fabricated device sizes were 1 and 10 mm^2. A comparison of *J–V* and *P–V* results is shown in Fig. 5, where LPCVD Si_3N_4 and LPCVD a-Si passivation demonstrate the highest power conversion efficiency at 17.12% and 16.16%, respectively. The improved efficiency originates primarily from an increase in V_{OC}, with relatively similar J_{SC} values. From the external quantum efficiency measurement, as shown in Fig. 6, the device structures, including the base thickness and antireflection layer, are well optimized for near-IR wavelength between 700 and 850 nm with above 80% eternal quantum efficiency (EQE) over this wavelength range. Dark *J–V* characteristics are shown in Fig. 7, with results from parameter extraction summarized in Table III. The LPCVD Si_3N_4 and a-Si passivation processes demonstrate a clear reduction in reverse saturation current and reduction in ideality factor from 1.968 to 1.4, demonstrating that the LPCVD processes are effectively passivating the deep

TABLE III
EXTRACTED PARAMETERS OF 10-mm^2 CELLS USING (1)

Passivation	J_0 (A/mm^2)	n
LPCVD Si_3N_4	5.31 x 10^{-12}	1.393
LPCVD a-Si	8.87 x 10^{-12}	1.419
Dry SiO_2	3.54 x 10^{-10}	1.851
PECVD Si_3N_4	7.03 x 10^{-11}	1.498
PECVD SiO_2	1.04 x 10^{-9}	1.943
Unpassivated	4.07 x 10^{-10}	1.968

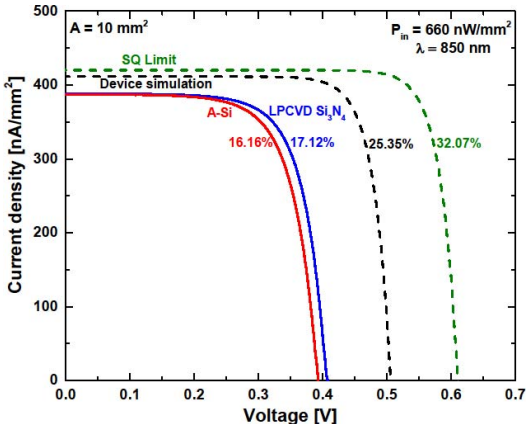

Fig. 8. Measured *J–V* characteristics and corresponding conversion efficiency and comparison with device simulation and SQ model.

sidewall with Si_3N_4 and a-Si. The improved dark *J–V* characteristics demonstrate a clear agreement with the measured improvements in V_{OC} for the Si_3N_4 and a-Si processes.

IV. DISCUSSION

The maximum efficiency achieved in the cells for this paper is 17.12% for the LPCVD Si_3N_4 under low-flux 850-nm LED illumination. This provides a power density of 113 nW/mm^2, above the desired value of 100 nW/mm^2 for mm-scale systems [8], [22]. The results are also improved over previously reported commercial cm-scale c-Si photovoltaic cells that were tested under the low-flux solar spectrum condition of 3000 nW/mm^2, with reported efficiency of 13.1% [14].

The limitation on power conversion efficiency of these cells is attributed to a reduction in V_{OC}, as shown in Fig. 8 comparing measured and simulated results. The evident reduction in measured V_{OC} in comparison to values obtained from the Shockley–Queisser (SQ) limit for Si [23], [24] and the drift-diffusion device simulation in Sentaurus device [18] arises from nonradiative recombination losses, including sidewall and surface recombination. The behavior of reduced V_{OC} is similar to reports on GaAs PV cells under low flux indoor illumination [11], [22]. As shown in Table IV, V_{OC} values and corresponding conversion efficiency decrease for the smaller 1-mm^2 devices, suggesting that sidewall recombination is more important for mm-scale applications in comparison with conventional cm-scale photovoltaic cells. Degradation in conversion efficiency under low incident light intensity by shunt resistance compared with the negligible impacts of series

TABLE IV
DEVICE SIZE DEPENDENCE ON DEVICE PARAMETERS OF LPCVD PASSIVATED CELLS UNDER ILLUMINATION OF 660 nw/mm^2 AT 850 nm

Passivation	LPCVD Si_3N_4		LPCVD a-Si	
Size (mm^2)	10	1	10	1
P/A (mm^{-1})	1.18	3.13	1.18	3.13
J_{SC} (nA/mm^2)	388.29	403.18	387.47	404.66
V_{OC} (V)	0.409	0.384	0.394	0.359
Efficiency (%)	17.12	15.91	16.16	15.53
J_0 (A/mm^2)	5.31x10^{-12}	2.36x10^{-11}	8.87x10^{-12}	1.45x10^{-11}
Ideality factor	1.393	1.502	1.419	1.356
Fill factor	0.711	0.678	0.699	0.705

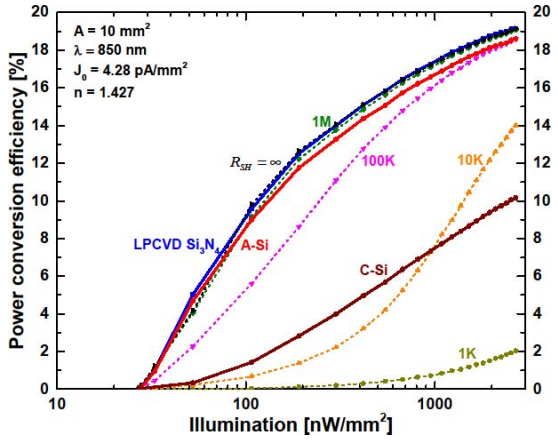

Fig. 9. Measured power conversion efficiency versus NIR illumination for varying device passivation and comparison with commercial c-Si. Simulated values using a diode model are shown assuming J_0 and *n* values shown in the inset and varying shunt resistance in (Ω-cm^2).

resistance [16], [17] can also impact the utility of PV cells for energy harvesting applications. Power conversion efficiency under variable intensity illumination was examined for the cells with LPCVD Si_3N_4 and a-Si passivation, as shown in Fig. 9. The measured devices exhibit a decrease in efficiency with reduced illumination, with similar behavior for both passivation techniques. Measured results for a commercial c-Si solar cell [32] with 22% power conversion efficiency under AM 1.5 illumination are shown for comparison, which exhibits a more dramatic decrease in efficiency with reduced illumination. To examine the possible influence of efficiency degradation due to shunt leakage, conversion efficiency was simulated using a diode model with variable shunt resistance and assuming extracted J_0 and n values from dark current measurement of tested cell. The LPCVD Si_3N_4 and a-Si passivated cells studied in this paper demonstrate a shunt resistance above 10 MΩ-cm^2, sufficient to prevent degradation in efficiency for the range of illumination studied. Efficiency degradation with illumination follows expected behavior, where cells are limited by the dark current (reverse saturation current density, J_0).

Further improvements in cell efficiency will, therefore, require reduction in J_0, where techniques, such as atomic layer deposition of Al_2O_3 [21], [25] and chemical surface treatments, including NH_4F [26], [27], $(NH_4)_2S$ [28], [29], and H_2S [30], [31], may be beneficial.

V. Conclusion

Small area Si photovoltaic cells were optimized based on simulation results for energy harvesting applications in the NIR transparency window of biological tissue between 700 and 1100 nm. High EQE above 80% and power conversion efficiency exceeding 17% are demonstrated under low-flux NIR illumination. The device performance was dramatically improved by incorporating a surface lightly doped emitter and LPCVD passivation. In contrast to conventional c-Si PV, the cells in this paper demonstrate stable performance under low illumination intensity that is limited by dark current rather than shunt leakage. The good performance of the small-area silicon cells under low illumination conditions is promising for through-tissue infrared energy harvesting, where further improvements may be achieved by additional measures to reduce recombination losses at interfaces.

References

[1] K. Murakawa, M. Kobayashi, O. Nakamura, and S. Kawata, "A wireless near-infrared energy system for medical implants," *IEEE Eng. Med. Biol. Mag.*, vol. 18, no. 6, pp. 70–72, Nov./Dec. 1999.

[2] K. Goto, T. Nakagawa, O. Nakamura, and S. Kawata, "An implantable power supply with an optically rechargeable lithium battery," *IEEE Trans. Biomed. Eng.*, vol. 48, no. 7, pp. 830–833, Jul. 2001.

[3] K. Bazaka and M. V. Jacob, "Implantable devices: Issues and challenges," *Electronics*, vol. 2, no. 1, pp. 1–34, 2013.

[4] J.-D. Kim, C. Sun, and I.-S. Suh, "A proposal on wireless power transfer for medical implantable applications based on reviews," in *Proc. IEEE Wireless Power Transf. Conf. (WPTC)*, May 2014, pp. 166–169.

[5] D. A. Borton, M. Yin, J. Aceros, and A. Nurmikko, "An implantable wireless neural interface for recording cortical circuit dynamics in moving primates," *J. Neural Eng.*, vol. 10, no. 2, p. 026010, 2013.

[6] K. D. Daniel, *et al.*, "Implantable diagnostic device for cancer monitoring," *Biosensors Bioelectron.*, vol. 24, no. 11, pp. 3252–3257, Jul. 2009.

[7] M. Z. Azad and M. Ali, "A miniaturized implantable antenna for GPS application," in *Proc. IEEE Antennas Propag. Soc. Int. Symp.*, Jul. 2006, pp. 1103–1106.

[8] Y. Lee *et al.*, "A modular 1 mm^3 die-stacked sensing platform with low power I^2C inter-die communication and multi-modal energy harvesting," *IEEE J. Solid-State Circuits*, vol. 48, no. 1, pp. 229–243, Jan. 2013.

[9] S. Roundy, P. K. Wright, and J. M. Rabaey, "Introduction," in *Energy Scavenging for Wireless Sensor Networks*. New York, NY, USA: Springer, 2004, pp. 1–26.

[10] A. N. Bashkatov, E. A. Genina, V. I. Kochubey, and V. V. Tuchin, "Optical properties of human skin, subcutaneous and mucous tissues in the wavelength range from 400 to 2000 nm," *J. Phys. D, Appl. Phys.*, vol. 38, no 15, p. 2543, Jul. 2005.

[11] A. S. Teran *et al.*, "Energy harvesting for GaAs photovoltaics under low-flux indoor lighting conditions," *IEEE Trans. Electron Devices*, vol. 63, no. 7, pp. 2820–2825, Jul. 2016.

[12] S. Ayazian, V. A. Akhavan, E. Soenen, ans A. Hassibi, "A photovoltaic-driven and energy-autonomous CMOS implantable sensor," *IEEE Trans. Biomed. Circuits Syst.*, vol. 6, no. 4, pp. 336–343, Aug. 2012.

[13] G. E. Bunea, K. E. Wilson, Y. Meydbray, M. P. Campbell, and D. M. De Ceuster, "Low light performance of mono-crystalline silicon solar cells," in *Proc. IEEE 4th World Conf. Photovolt. Energy Conf.*, vol. 2. May 2006, pp. 1312–1314.

[14] N. H. Reich *et al.*, "Crystalline silicon cell performance at low light intensities," *Solar Energy Mater. Solar Cells*, vol. 93, no. 9, pp. 1471–1481, 2009.

[15] T. B. Stellwag *et al.*, "Effects of perimeter recombination on GaAs-based solar cells," in *Proc. Conf. Rec. 21st IEEE Photovolt. Specialists Conf.*, May 1990, pp. 442–447.

[16] O. Breitenstein, J. P. Rakotoniaina, M. H. Al Rifai, and M. Werner, "Shunt types in crystalline silicon solar cells," *Progr. Photovolt. Res. Appl.*, vol. 12, no. 7, pp. 529–538, Nov. 2004.

[17] K. Rühle, M. Freunek, L. M. Reindl, and M. Kasemann, "Designing photovoltaic cells for indoor energy harvesting systems," in *Proc. 9th Int. Multi-Conf. Syst. Signals Devices (SSD)*, pp. 1–5, Mar. 2012.

[18] *Guide Sentaurus Device User and E. Version*, Synopsys Inc., Mountain View, CA, USA, 2013.

[19] M. A. Green and M. J. Keevers, "Optical properties of intrinsic silicon at 300 K," *Prog. Photovolt. Res. Appl.*, vol. 3, no. 3, pp. 189–192, 1995.

[20] C. Riordan and R. Hulstron, "What is an air mass 1.5 spectrum? (solar cell performance calculations)," in *Proc. Conf. Rec. 21st IEEE Photovolt. Specialists Conf.*, May 1990, pp. 1085–1088.

[21] K. Rühle *et al.*, "Passivation layers for indoor solar cells at low irradiation intensities," *Energy Procedia*, vol. 27, pp. 406–411, Apr. 2012.

[22] A. S. Teranet *et al.*, "AlGaAs photovoltaics for indoor energy harvesting in mm-scale wireless sensor nodes," *IEEE Trans. Electron Devices*, vol. 62, no. 7, pp. 2170–2175, Jul. 2015.

[23] W. Shockley and H. J. Queisser, "Detailed balance limit of efficiency of $p-n$ junction solar cells," *J. Appl. Phys.*, vol. 32, no. 3, pp. 510–519, 1961.

[24] O. D. Miller, E. Yablonovitch, and S. R. Kurtz, "Strong internal and external luminescence as solar cells approach the shockley–queisser limit," *IEEE J. Photovolt.*, vol. 2, no. 3, pp. 303–311, Jul. 2012.

[25] B. Hoex, J. Schmidt, P. Pohl, M. C. M. van de Sanden, and W. M. M. Kessels, "Silicon surface passivation by atomic layer deposited Al_2O_3," *J. Appl. Phys.*, vol. 104, no. 4, p. 044903, 2008.

[26] H. Angermann *et al.*, "Wet-chemical passivation of atomically flat and structured silicon substrates for solar cell application," *Appl. Surf. Sci.*, vol. 254, no. 12, pp. 3615–3625, Apr. 2008.

[27] H. Angermann, W. Henrion, M. Rebien, and A. Röseler, "Wet-chemical passivation and characterization of silicon interfaces for solar cell applications," *Solar Nergy Mater. Solar Cells*, vol. 83, no. 4, pp. 331–346, Jul. 2004.

[28] G. Song, M. Y. Ali, and M. Tao, "A high Schottky-barrier of 1.1 eV between Al and S-passivated p-type Si(100) surface," *IEEE Electron Device Lett.*, vol. 28, no. 1, pp. 71–73, Jan. 2007.

[29] M. Y. Ali and M. Tao, "Effect of sulfur passivation of silicon (100) on Schottky barrier height: Surface states versus surface dipole," *J. Appl. Phys.*, vol. 101, no. 10, p. 103708, 2007.

[30] H.-F. Zhang, A. Saha, W.-C. Sun, and M. Tao, "Characterization of Al/Si junctions on Si(100) wafers with chemical vapor deposition-based sulfur passivation," *Appl. Phys. A*, vol. 116, no. 4, pp. 2031–2038, 2014.

[31] A. Saha, H. Zhang, W.-C. Sun, and M. Tao, "Grain boundary passivation in multicrystalline silicon using hydrogen sulfide," *ECS J. Solid State Sci. Technol.*, vol. 4, no. 7, P186–P189, 2015.

[32] *IXYS Corporation: KXOB22-12X1*. (2010). [Online]. Available: https://docs.google.com/viewerng/viewer?url=http://ixapps.ixys.com/DataSheet/KXOB22-12X1L-DATA-SHEET-20130902-.pdf

Eunseong Moon (S'16) received the B.S. degree in electrical engineering from the Chung-Ang University, Seoul, South Korea, in 2012, and the M.S. degree in electrical engineering from the University of Michigan, Ann Arbor, MI, USA, in 2015, where he is currently pursuing the Ph.D. degree.

His current research interests include photovoltaic energy harvesting for mm-scale systems.

David Blaauw (SM'07–F'12) received the B.S. degree in physics and computer science from Duke University, Durham, NC, USA, in 1986, and the Ph.D. degree in computer science from the University of Illinois at Urbana–Champaign, Urbana, IL, USA, in 1991.

Since 2001, he has been with the Faculty, University of Michigan, Ann Arbor, MI, USA, where he is currently a Professor.

Jamie D. Phillips (M'01–SM'06) received the B.S., M.S., and Ph.D. degrees in electrical engineering from the University of Michigan, Ann Arbor, MI, USA.

He was with the Faculty, University of Michigan in 2002, where he is currently an Arthur F. Thurnau Professor. His current research interests include compound semiconductor and oxide-based materials for optoelectronics and electronics.